

Single-mode antiresonant terahertz fiber based on mode coupling between core and cladding

Shuai Sun(孙帅), Wei Shi(史伟), Quan Sheng(盛泉), Shijie Fu(付士杰), Zhongbao Yan(闫忠宝), Shuai Zhang(张帅), Junxiang Zhang(张钧翔), Chaodu Shi(史朝督), Guizhong Zhang(张贵忠), and Jianquan Yao(姚建铨)

Citation: Chin. Phys. B, 2021, 30 (**12**): 124205. DOI: 10.1088/1674-1056/ac032e
Journal homepage: http://cpb.iphy.ac.cn; http://iopscience.iop.org/cpb

What follows is a list of articles you may be interested in

High-efficiency terahertz wave generation with multiple frequencies by optimized cascaded difference frequency generation

Zhongyang Li(李忠洋), Binzhe Jiao(焦彬哲), Wenkai Liu(刘文锴), Qingfeng Hu(胡青峰), Gege Zhang(张格格), Qianze Yan(颜钤泽), Pibin Bing(邴丕彬), Fengrui Zhang(张风蕊), Zhan Wang(王湛), and Jianquan Yao(姚建铨)
Chin. Phys. B, 2021, 30 (**4**): 044211. DOI: 10.1088/1674-1056/abe3eb

Modulation and enhancement of photonic spin Hall effect with graphene in broadband regions

Peng Dong(董鹏), Gaojun Wang(王高俊), and Jie Cheng(程杰)
Chin. Phys. B, 2021, 30 (**3**): 034202. DOI: 10.1088/1674-1056/abccb2

Efficient manipulation of terahertz waves by multi-bit coding metasurfaces and further applications of such metasurfaces

Yunping Qi(祁云平) Baohe Zhang(张宝和), Jinghui Ding(丁京徽), Ting Zhang(张婷), Xiangxian Wang(王向贤), and Zao Yi(易早)
Chin. Phys. B, 2021, 30 (**2**): 024211. DOI: 10.1088/1674-1056/abd6fc

Theoretical research on terahertz wave generation from planar waveguide by optimized cascaded difference frequency generation

Zhongyang Li(李忠洋), Jia Zhao(赵佳), Wenkai Liu(刘文锴), Qingfeng Hu(胡青峰), Yongjun Li(李永军), Binzhe Jiao(焦彬哲), Pibin Bing(邴丕彬), Hongtao Zhang(张红涛), Lian Tan(谭联), and Jianquan Yao(姚建铨)
Chin. Phys. B, 2021, 30 (**2**): 024209. DOI: 10.1088/1674-1056/abc3b7

Plasmonic characteristics of suspended graphene-coated wedge porous silicon nanowires with Ag partition

Xu Wang(王旭), Jue Wang(王珏), Tao Ma(马涛), Heng Liu(刘恒), and Fang Wang(王芳)
Chin. Phys. B, 2021, 30 (**1**): 014207. DOI: 10.1088/1674-1056/abb65c

---

Single-mode antiresonant terahertz fiber based on mode coupling between core and cladding*

Shuai Sun(孙帅)[1,2], Wei Shi(史伟)[1,2,†], Quan Sheng(盛泉)[1,2], Shijie Fu(付士杰)[1,2], Zhongbao Yan(闫忠宝)[1,2], Shuai Zhang(张帅)[1,2], Junxiang Zhang(张钧翔)[1,2], Chaodu Shi(史朝督)[1,2], Guizhong Zhang(张贵忠)[1,2], and Jianquan Yao(姚建铨)[1,2]

[1] *Institute of Laser and Optoelectronics, School of Precision Instrument and Optoelectronics Engineering, Tianjin University, Tianjin* 300072, *China*

[2] *Key Laboratory of Optoelectronic Information Science and Technology (Ministry of Education), Tianjin University, Tianjin* 300072, *China*

(Received 19 April 2021; revised manuscript received 14 May 2021; accepted manuscript online 20 May 2021)

Based on the index-induced mode coupling between the higher-order mode in core and the fundamental mode in cladding tubes, the single-mode operation can be realized in any antiresonant fibers (ARFs) when satisfying that the area ratio of cladding tube and core is about 0.46:1, and this area ratio also should be modified according to the shape and the number of cladding tubes. In the ARF with nodal core boundary, the mode in core also can couple with the mode in the wall of core boundary, which can further enhance the suppression of high-order mode. Accordingly, an ARF with conjoint semi-elliptical cladding tubes realizes a loss of higher-order mode larger than 30 dB/m; simultaneously, a loss of fundamental mode loss less than 0.4 dB/m.

Keywords: terahertz, mode coupling, single-mode fiber

PACS: 42.81.Qb, 42.81.–i, 95.85.Gn **DOI:** 10.1088/1674-1056/ac032e

1. Introduction

Terahertz (THz) waves locate between the far-infrared wave and microwave ranges of the electromagnetic spectrum. Earlier, this region used to be an academic blank, baffling researchers for decades. THz technology has developed rapidly and gained significance for the extensive research on THz radiation sources and detector devices. THz waves possess many unique properties, such as high penetrability into nonpolar materials and low photon energy, which promote nondestructive testing and bio-imaging.[1] High-performance THz waveguides are still in research, and the applications of THz waves are primarily based on the free-space optical path, which is inefficient and may import errors caused by the absorption of water vapor. To the best of our knowledge, almost all optical materials considerably absorb THz waves. The high material losses prevent the solid-core fiber from becoming an acceptable THz waveguide. However, the antiresonant fiber (ARF) guiding the light in the air core can weaken the effect from material absorption and achieve low-loss THz wave transmission.[2,3]

The shell of the cladding tube is the key factor affecting the light transmission in ARF. In ARF, the cladding tube's shell acts like the antiresonant wall in the slab waveguide, making each cladding tube an antiresonant element.[4,5] In ARFs, for the antiresonance of cladding tubes, light is confined to the central air core. Only the material absorption loss at the surface contributes to the efficiency of the material absorption loss. In 2018, Gao[6] demonstrated a silica ARF with conjoined tube cladding for infrared waves, obtaining a transmission loss of 2 dB/km, the lowest transmission of ARF reported so far. Thus, it is expected to break the transmission limit of silica fiber by using the ARF. The separation between light and fiber material also guarantees the ARF a high laser-induced damage threshold; therefore, the ARF is suitable as the reaction cell for optically pumped gas fiber lasers. In 2010, Nampoothiri presented an optically pumped ethyne (C_2H_2) gas mid-infrared fiber laser utilizing the hollow-core fiber as the reaction gas cell and successfully obtained a 3.1-μm optically pumped gas fiber laser. Subsequently, several reaction gases were applied to broaden the output spectrum of the fiber laser.[7,8] In 2018, a 100-m ARF serving as the reaction cell and a mid-infrared fiber laser with an output of the magnitude of watts was achieved.[5] At present, ARF investigations focus mainly on the redesign of cladding tubes to improve fiber performance or realize special abilities such as birefringence and single mode.[9–13]

The most commonly used material for visible and infrared ARFs is fused silica, which causes significant absorption loss of THz waves.[14] A few polymer materials, such as polypropylene (PP), high-density polyethylene (HDPE),

*Project supported by the National Natural Science Foundation of China (Grant No. 62075159), the National Key Research and Development Program of China (Grant No. 2017YFF0104603), the 111 Project of China (Grant No. B17031), and the Major Scientific and Technological Innovation Projects of Key Research and Development Plans in Shandong Province, CHina (Grant No. 2019JZZY020206).

†Corresponding author. E-mail: shiwei@tju.edu.cn

© 2021 Chinese Physical Society and IOP Publishing Ltd

cyclic olefin copolymers (COC), and polymethyl-pentene (PMP; brand name: TPX).[15] Theoretical research indicates that with low-loss polymer material, the transmission loss of THz ARFs can be dozens of times lower than that of solid-core fibers.[16] In 2020, Islam reviewed the optimal materials, the guiding mechanisms, the fabrications, and the applications of various THz optical fibers; then confirmed that ARF could provide low-loss THz guidance and comparatively simple fabrication.[17] Outstanding mechanical properties and thermoplasticity make polymer materials a feasible selection for fabricating high-performance THz waveguides. In 2014, Ji proposed a porous microstructured THz fiber based on COC material; furthermore, a high-quality fiber preform was manufactured by the hot extrusion molding method and then drawn into fiber through a unique draw tower.[18] It can also fabricate the ARF preform using the stack-and-draw method[19,20] and the direct extrusion method.[21] Further, three-dimensional (3D) printing technology has also accelerated the realization of complex microstructured THz fibers.[22–24]

Considering the remarkable suppression of the polarization mode dispersion (PMD) and mode noise, single-mode fibers play a significant role in THz applications; however, there have been few comprehensive studies on single-mode THz ARFs. In 2015, Uebel proposed a single-mode hollow-core fiber achieved by the higher-order mode (HOM) filter. And then, they numerically and experimentally proved that the single-mode could occur when the diameter ratio of capillaries inside the central hollow core was approximately 0.68; besides, this single-mode guidance was demonstrated in all the wavelength ranges.[25] In 2016, Habib proposed a single-mode ARF based on anisotropic cladding tubes, and then the HOM suppression was significantly improved by using symmetrically distributed anisotropic cladding tubes.[9] In 2016, Yu designed and fabricated a hollow-core ARF with seven special cladding tubes, and the experimental results indicated single-mode characteristics.[26] In 2017, Edavalath proposed a single-mode ARF produced by geometrically twisting the fiber. The effective axial propagation constant of the fundamental mode increased and, simultaneously, the HOM was remarkably suppressed.[27] In 2019, Habib demonstrated that the geometrical structure and the number of antiresonant cladding tubes could strongly impact the HOM contents.[28] In 2020, Yan proposed a double-layer-cladding ARF, and by adjusting the diameters of two layers of cladding tubes, three broad-band single-polarization single-mode regions were achieved.[29] Our previous study has done a preliminary investigation on the HOM suppression of THz ARF.[30] In this study, the single-mode THz ARF is comprehensively investigated based on the mode coupling between the core and the cladding. Then we discussed the method of promoting single-mode performance.

2. Fiber design and numerical simulations

The guidance mechanism of ARF is well understood. In ARF, the thin shell of the periodic cladding tube has an inherent resonant period. When the wavelength of incident light is lying in this period, the incident light will resonate with the cladding tubes, causing ultrahigh transmission loss. On the contrary, when the wavelength of incident light is far from this resonant period, the cladding tubes will exclude the incident light coupling into the cladding. The confinement loss (CL) is the main contributor to the transmission loss of ARF; which can calculate using the formula

$$\mathrm{CL} = \frac{20}{\ln 10}\frac{2\pi f}{c}N_i, \tag{1}$$

where c is the velocity of light, f is the frequency of incident light, and N_i is the imaginary part of the effective refractive index. In this study, the transmission characteristics of ARFs with different cladding tubes are investigated based on the finite-element-method software — COMSOL Multiphysics.

The 1.89-THz laser lies in the primary output spectrum of the optically pumped difluoromethane (CH_2F_2) THz laser; for this laser, the COC material has a complex refractive index of $1.531 + 0.00175\mathrm{i}$.[15] We proposed an ARF with round cladding tubes (R-ARF) based on COC material for this laser, and figure 1(a) presents the cross-sectional diagram of the fiber. The R-ARF is composed of six round tubes inserted inside the extramural cladding. The cladding tube's inner and outer diameters are denoted by d and D, respectively, and its shell thickness is denoted by T. The size of the fiber core directly determines the transmission loss; thus, the diameter of the fiber core, D_{core}, is maintained at 2000 μm. In the simulation, the shell thickness of extramural cladding keeps at 500 μm. The confinement loss of fundamental mode ($\mathrm{CL_F}$) varying with D and T is depicted in Fig. 1(d). The simulation results indicate that this THz fiber has a significant antiresonant effect, which is mainly determined by T, and cladding tubes need enough size to expose the antiresonant effect. The electric field distributions of the fiber in resonant and antiresonant status, presented in Figs. 1(b) and 1(c), demonstrate that when the fiber is in resonant state, light couples to a large extent with the cladding tubes and extramural cladding; however, when the fiber is in an antiresonant state, the cladding tubes operate like reflectors resisting the light coupling. When $D = 1.2$ mm, $\mathrm{CL_F}$ varying with T is depicted as the solid curve in Fig. 1(d). It can be seen, with the increase in T, $\mathrm{CL_F}$ exhibits a periodic change at 70 μm. $\mathrm{CL_F}$ exhibits an increasing trend with the increase in T caused by the material absorption in each optimal antiresonant status. When the ARF is in the first antiresonant period, the minimum $\mathrm{CL_F}$ is about 0.1 dB/m, which is approximately 0.7 dB/m when the ARF is in the fourth antiresonant period.

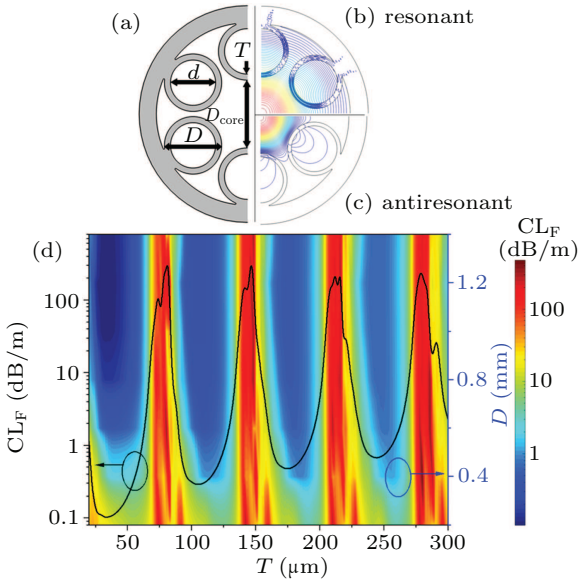


Fig. 1. (a) Cross-sectional diagram of R-ARF. Electric field distribution diagrams of fibers in (b) resonant and (c) antiresonant status. (d) CL_F varying with T and D. Solid curve is the CL_F varying with T when D is 1.2 mm.

2.1. ARF with round cladding tubes

In the ARF with single-layer cladding tubes, investigations proved that when the ratio of the internal diameter of the cladding tubes to the core diameter is approximately 0.682:1, the HOM in the central core strongly couples with the fundamental mode (FM) in the cladding tubes, causing an abnormally high CL of the HOM (CL_H).[25] In this study, the mode coupling in THz ARF has been studied thoroughly, based on the R-ARF, as presented in Fig. 1(a). To facilitate the numerical calculation, T is maintained at 104 μm, leading the fiber to be in the second optimal antiresonant status. Figures 2(a) and 2(b) depict the light guidance properties of R-ARF under geometric deformation of cladding tubes. It indicates that the geometric deformation has a significant impact on HOM's loss but barely on CL_F (HE11 mode). Figures 3(a)–3(e) depict the electric field distributions of HE11 mode, TE01 mode, HE21 mode, and TE01 supermodes.

The simulation results indicate that the TE01 mode has the lowest transmission loss among the HOMs, and in this study, the TE01 mode represented the HOM. With the increase in d from 1000 μm to 1500 μm, CL_F remains almost unchanged at 0.3 dB/m; conversely, CL_H appears to exhibit an abnormal growth, forming a specific suppression of the HOM in the THz wave guidance. When d is in the range of 1320 μm–1380 μm, CL_H is more significant than 3 dB/m, and it reaches a maximum value of 7.4 dB/m when $d = 1355$ μm. This mode coupling between the core and cladding results in suppressing the HOM; after that, the ARF can realize excellent single-mode properties. It is noteworthy that the N_r of the HOM grossly decreases with d, and when the ARF is in the HOM suppression status, the N_r of the HOM exhibits an abnormal variation. An ARF with dual-layer cladding tubes (dual-layer ARF) and a pipe with an inner diameter of d are proposed as control groups in this study, as illustrated in Fig. 2(a), and the nested cladding tubes of dual-layer ARF can suppress the cladding mode. As the control group, this dual-layer ARF has the same geometric parameters with R-ARF; besides, the nest cladding tube has a shell thickness of T and an inner diameter of $d/2$. As indicated by the blue dotted line in Fig. 2(b), in the ARF with dual-layer cladding tubes, the N_r of the TE01 mode displays a linear reduction, which is the reference database for R-ARF and confirms the abnormal variation of the HOM in R-ARF.

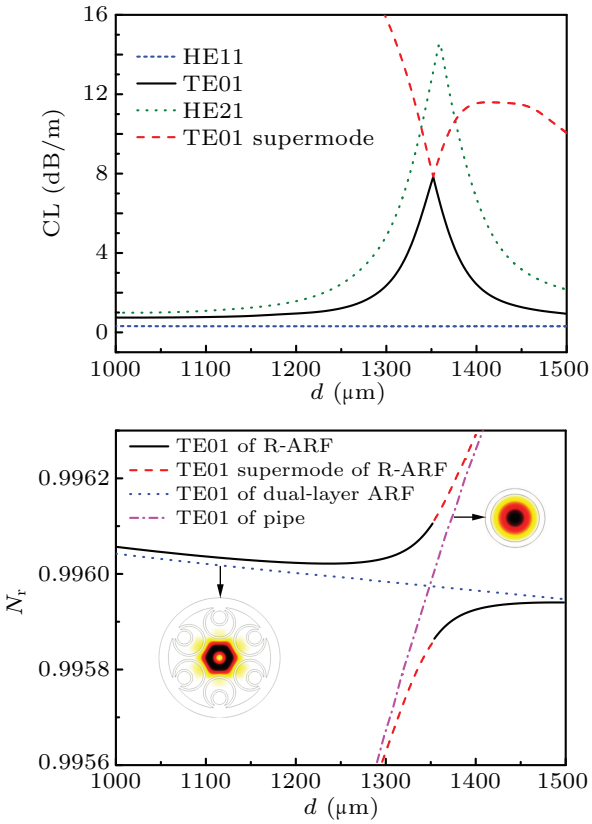


Fig. 2. (a) CL of FM and HOMs varying with d in R-ARF. (b) Varying with d, the N_r of HOMs in R-ARF, and N_r of TE01 mode in dual-layer ARF, and N_r of HE11 mode in the pipe. Pipe and dual-layer ARF are illustrated.

In the simulation, when R-ARF has an apparent HOM suppression, there are two fiber TE01 supermodes, which have a relatively strong HE11 mode in the cladding and a weak TE01 mode in the core. The red dashed lines in Figs. 2(a) and 2(b), indicated the loss and the N_r of TE01 supermodes. Besides, as indicated by the purple dotted–dashed line in Fig. 2(b), in the pipe, N_r of HE11 mode displays a linear growth, which is the reference database for fiber TE01 supermodes. When R-ARF approaches the optimal HOM suppression status, TE01 mode and TE01 supermode tend to be the same, distinguished as TE01 supermode (core) and TE01 supermode (cladding) based on the intensity of the mode in the cladding. The electric field distributions of the TE01 supermodes when $d = 1350$ μm and 1360 μm are displayed in

Fig. 3(e), which illustrated that when the R-ARF is in the optimal HOM suppression status, the HOM in the core and FM in the cladding coexist. It can infer that there are mutual conversions of TE01 (core) and TE01 (cladding) with change in d.

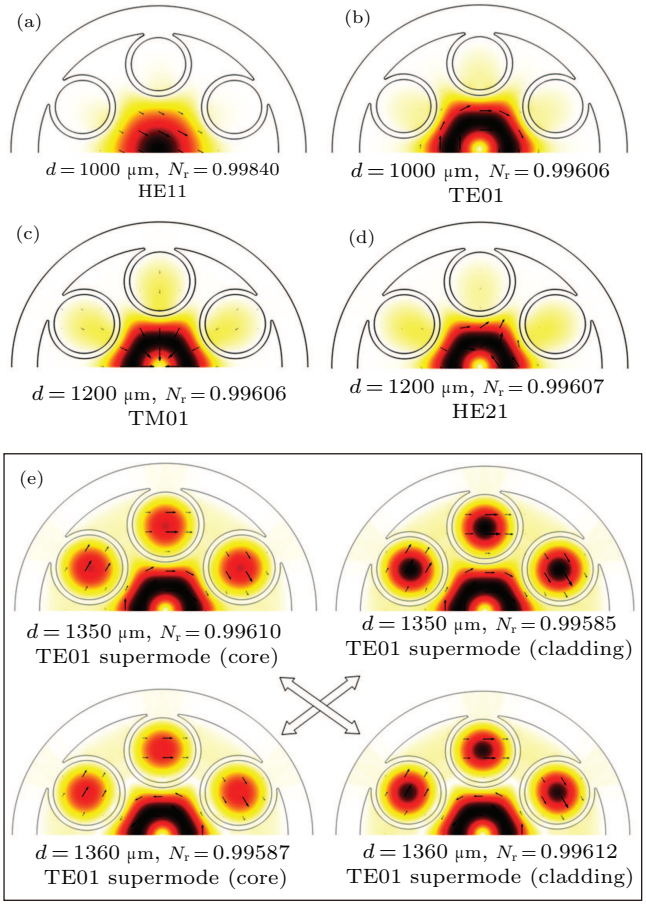


Fig. 3. Electric field distributions of R-ARF under different status: (a) HE11 mode, (b) TE01 mode, (c) TM01 mode, (d) HE21 mode, and (e) TE01 supermodes; arrows indicate electric field lines.

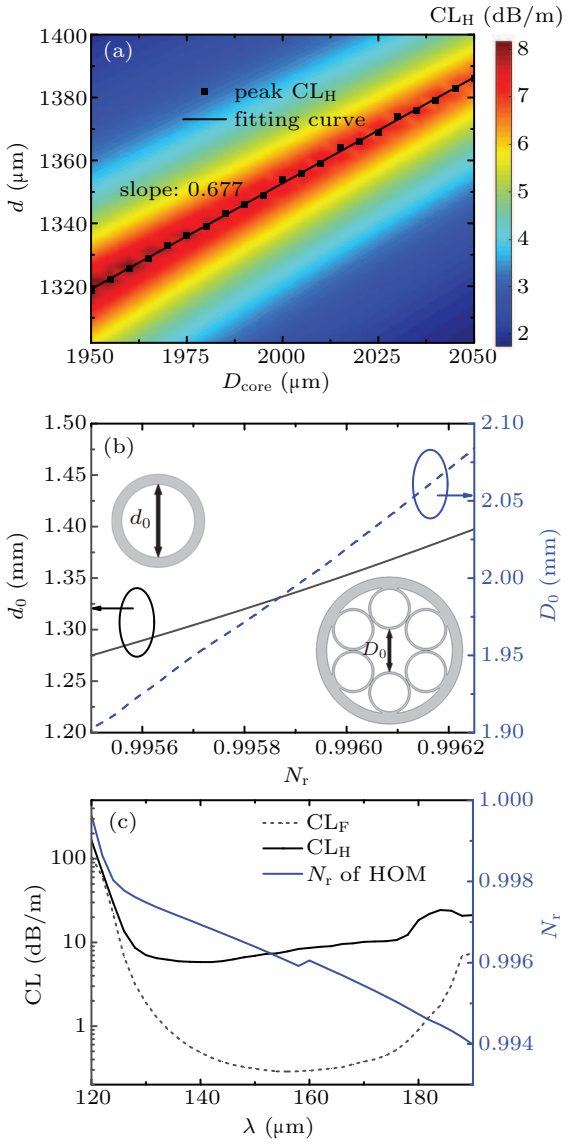


Fig. 4. In R-ARF, CL_H as a function of D_{core} and d. Black squares indicate peak points of CL_H, and the black line indicates the fitting curve. (b) N_r of FM in the thin-shell pipe varying with diameter, and N_r of HOM in the close-packed-tubes ARF varying with diameter. (c) In R-ARF, transmission characteristics vary with the wavelength of the incident wave.

The inner diameters of the cladding tubes and central air core are varied simultaneously, and figure 4(a) depicted the CL_H as a function of D_{core} and d. The peak values of CL_H corresponding to different values of d and D_{core} exhibit a linear distribution. Excluding the limited precision of the simulation calculations, the fitting curve of the peak CL_H illustrates that the critical factor that determines the suppression of the HOM in the R-ARF is the rate of d to D_{core}; meanwhile, when this rate is approximately 0.677:1, the R-ARF realizes the optimal suppression of the HOM. Besides, when R-ARF realizes the optimal HOM suppression, the cross-sectional area ratio of cladding tubes and central air core is about 0.458:1. To further investigate the mode coupling between core and cladding, this paper proposed a thin-shell pipe with an internal diameter of d and a six-close-packed-tube ARF with a core diameter D. The thin-shell pipe has the same thickness as the cladding tubes of the six-close-packed-tube ARF.

The simulation indicates that the ARF with six closed-packed cladding tubes exhibits no suppression of the HOM. As presented in Fig. 4(b), with the changes in d and D, the N_r of FM in the thin-shell tube has a series of intersection points with the N_r of the HOM in the close-packed-tube ARF. With the change of d and D, the N_r of FM in the thin-shell pipe and the N_r of HOM in the close-packed-tubes ARF are depicted in Fig. 4(b). D and d change respectively, and N_r of FM in the thin-shell pipe has series of intersection values with the N_r of HOM in the close-packed-tubes ARF, such as when d is about 1.29 mm, and when D is 1.925 mm, two waveguides have the same N_r of 0.9956. The thin-shell pipe acts like the cladding tube of the ARF, and the intersection point in Fig. 4(b) represents the phase match of the FM in the cladding with the HOM in the core. Moreover, the intersection point distributions (d, D) in Fig. 4(b) coincide with the fitting curve distribution (d, D_{core}) presented in Fig. 4(a). It can conclude that the

index-induced phase match between core and cladding leads to the mode coupling between the core and cladding, which affords ARF an HOM-suppression ability. When T maintains at 104 μm and d at 1360 μm, CL_F and CL_H varying with the incident wave wavelength, λ, are depicted in Fig. 4(c). It can be seen this ARF has a flat transmission window in broad-band; furthermore, the HOM suppression is always effective in the transmission windows.

2.2. ARF with semi-elliptical cladding tubes

Extending the contact area of the cladding mode with extramural cladding can lead to the consumption of the HOM. Thus, a compact ARF with semi-elliptical cladding tubes (S-ARF), as illustrated in Fig. 5(a), is proposed to develop a higher-performance single-mode ARF. In S-ARF, R_a and R_b represent the major and minor axis radii of the cladding tubes. The extramural cladding shrinks and covers part of the cladding tubes by D_c, shaping the cladding tubes into semi ellipse. When R_a and R_b are 1200 μm and 1000 μm, respectively, the simulation result indicates that with the increase in D_c, the CL_F increases only slightly from 0.33 dB/m to 0.34 dB/m; simultaneously, CL_H appears to be varying more drastically than that in R-ARF.

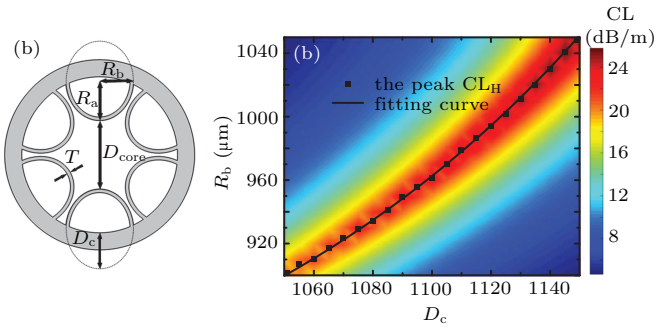


Fig. 5. (a) Cross-sectional diagram of S-ARF. (b) CL_H as a function of D_c and R_b. Black squares represent peak points of CL_H, and the black line represents the fitting curve.

To further study the key factors affecting the mode coupling in S-ARF, R_a is varied from 900 μm to 1050 μm, and D_c is varied from 1050 μm to 1150 μm. The CL_H is depicted in Fig. 5(b) as a function of D_c and R_a, demonstrating that in a wide geometric deformation range of cladding tubes, the S-ARF could achieve a high CL_H. The enlargement of cladding tubes in the ring direction of the fiber cross-section effectively enforces the suppression of the HOM. Shrinking the cladding from elliptical tubes to semi-elliptical tubes just slightly sacrifices the transmission performance of the FM. Moreover, the semi-elliptical cladding tubes provide a large contact area for the cladding mode with the extramural cladding, which significantly exacerbates the consumption on the HOM, and, finally, the CL_H was improved to more than 24 dB/m. When ARF has an optimal single-mode operation, the cross-sectional area ratio of cladding tubes and central air core is about 0.5:1.

2.3. Single-mode ARF with positive-curvature core

Our previous study[30] has confirmed that the single-operation condition can be achieved in the ARFs with round cladding tubes, elliptical cladding tubes, and semi-elliptical cladding tubes based on the HOM suppression. Integrating with the investigations in this paper, it can speculate that the ARF can realize the single-mode operation by keeping the cross-sectional area ratio of core and cladding tube at 0.46:1. Meanwhile, that area ratio should be modified according to the number and the shape of cladding tubes. We proposed a simple-structured ARF with a positive-curvature core boundary to verify this speculation, as illustrated in Fig. 6(a). And this positive-curvature ARF comprises two inner and external cladding tubes, which are linked by several borders. When the cladding tube number, N, is varied from 6 to 8, and T is 106 μm, the values of CL_F and CL_H varying with L are depicted in Figs. 6(c) and 6(d). When N is varied from 6 to 8, the area ratio of cladding tubes and core for optimal HOM suppression is 0.47:1, 0.44:1, and 0.415:1, respectively. Consistent with the previous speculation, this simple-structured ARF can realize a single-mode operation by adjusting the cross-sectional area ratio of cladding tubes and core. But for the existence of the conjoint points, the mode in the central air core is consumed distinctly.

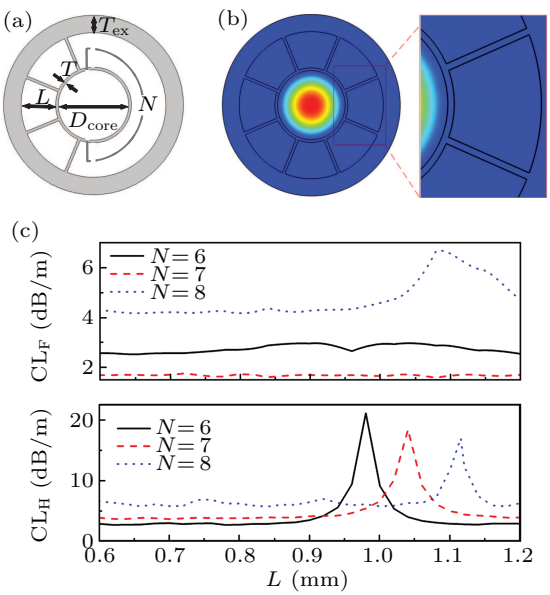


Fig. 6. (a) Cross-sectional diagram of the ARF with positive-curvature core. (b) Electric field distribution of the FM in the ARF with $N = 8$. In the fiber with different N, the values of CL_F (b) and CL_H (c) varying with L.

It is worth noting that, in Fig. 6(c), the CL_F of the ARF with $N = 8$ appears an abnormal increase when L approaches 1.1 mm. The electric field distribution of the FM in the ARF with $N = 8$ is depicted in Fig. 6(b), and it demonstrated that the FM in core can slightly couple with the mode in the wall of core boundary, which increases the value of CL_F. It can be seen, this coupling between core and the mode in the wall of

core boundary is related to the cladding tube number and the size of cladding tube.

2.4. Single-mode ARF with negative-curvature core

In single-mode S-ARF, the gaps between cladding tubes are small, which difficult the manufacture. The conjoint points among cladding tubes are confirmed to affect the transmission loss of fiber,[14] and the conjoint cladding tubes have the potential for FM suppression and HOM suppression. In this paper, we optimized the nodeless cladding tubes of S-ARF into nodal cladding tubes and proposed a nodal S-ARF as illustrated in Fig. 7(a). In nodal S-ARF, the core diameter, D_{core}, is maintaining at 2 mm, and the round tubes have a diameter of d and a shell thickness of T. The round tubes conjoin with each other and forming a common wall, besides, simultaneously, numbers of thin walls with a length of L and a thickness of T link the common borders with the external cladding. In nodal S-ARF with 6 cladding tubes, the value of CL_{H} as a function of d and L is depicted in Fig. 7(b), demonstrating that the structural deformation of cladding tubes could significantly affect the loss of HOM. The nodal S-ARF can achieve the highest CL_{H} about 28 dB/m which is higher than that of S-ARF by deforming the cladding tubes. What is noteworthy is that, when d is 2.2 mm, there is an obvious fault in the distribution of peak value in Fig. 7(b). In this fault, the value of CL_{H} is smooth and more significant than 10 dB/m when L is varied from 0.2 mm to 0.6 mm. When deforming the cladding tubes of ARF, the value of CL_{F} is depicted in Fig. 7(c), and there are two distinct high loss bands when D is 2.18 mm and 2.3 mm, which have no effect on the single-mode characteristic of fiber.

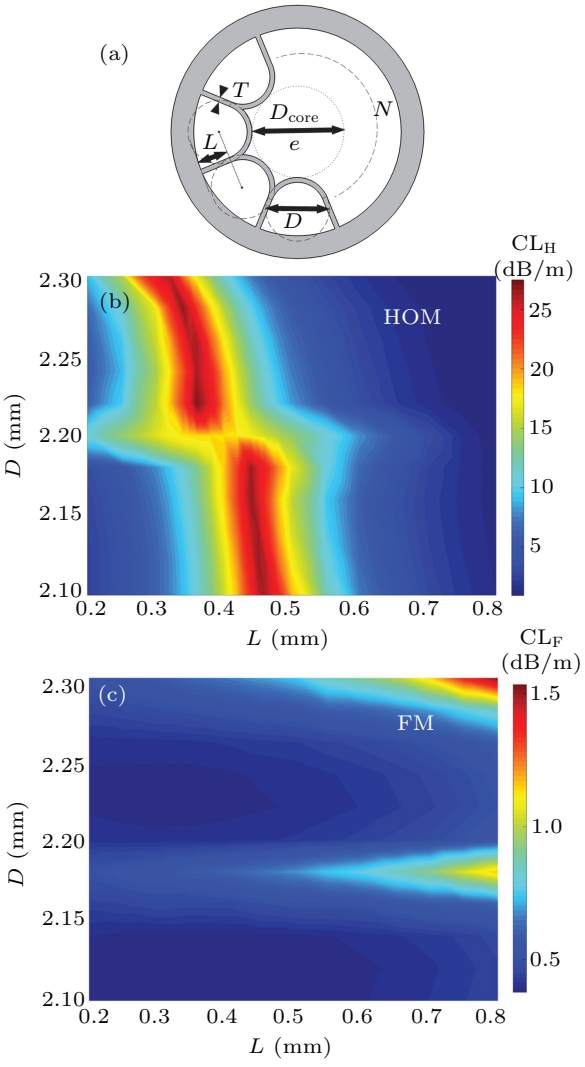


Fig. 7. (a) Cross-sectional diagram of the ARF with a positive-curvature core. In the fiber with different numbers of cladding tubes, the values of CL_{F} (b) and CL_{H} (c) varying with L.

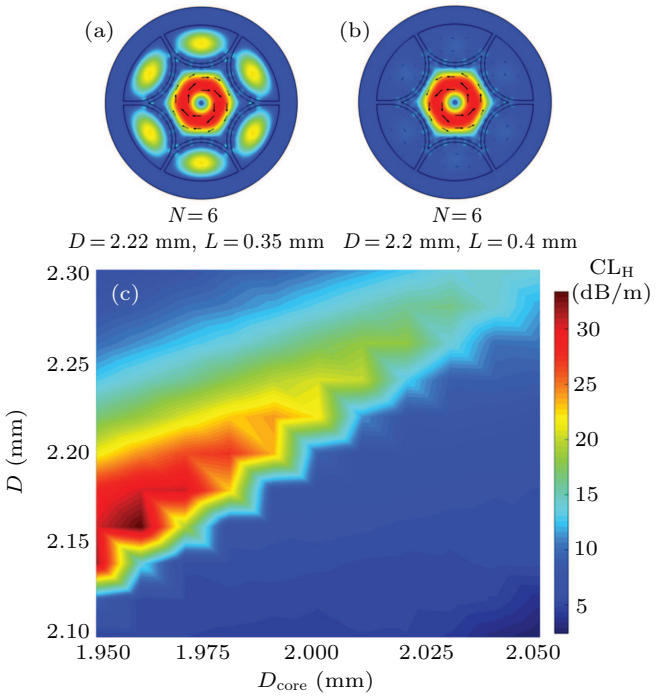


Fig. 8. (a) The electric field distributions of HOM when $L = 0.35$ mm, $D = 2.22$ mm, and (b) when $L = 0.45$ mm, $D = 2.2$ mm. (c) In the nodal S-ARF with 6 cladding tubes, CL_{H} as a function of D and D_{core}.

In the nodal S-ARF with 6 cladding tubes, when d is 2.22 mm, and L is 0.35 mm, fiber has an optimal suppression on HOM, and figure 8(a) depicts the electric field distribution of nodal S-ARF. It can be seen that the mode in core couples with the mode in cladding tubes, as well couples with the mode in core boundary (core boundary mode). In this nodal S-ARF, the coupling of core mode and the core boundary mode is always simultaneous with the coupling of core mode and cladding modes which endows fiber an additional suppression on HOM. When d is 2.2 mm, and L is 0.45 mm, the electric field distribution of the nodal S-ARF is depicted in Fig. 8(b). It demonstrates that the core mode forcefully couples with the core boundary mode, which impedes the coupling of core mode and the mode in cladding tubes. When L is 0.45 mm, the value of CL_{H} as a function of D_{core} and D is depicted in Fig. 8(c), and there is an obvious value contrast of CL_{H}. In Fig. 8(c), the value contrast of CL_{H} distributes linearly; and it demonstrates that the coupling between the core mode and core boundary mode is strongly affected by the diameter ratio of D_{core} and D.

When the cladding tube number of nodal S-ARF, N, is donated at 7 and 8, the values of CL_H as functions of D and L are depicted in Figs. 9(a) and 9(b). Both the nodal S-ARFs with 7 and 8 cladding tubes can achieve an excellent suppression for HOM. Furthermore, the HOM suppression is mainly affected by L. Besides, in the nodal S-ARF with 7 cladding tubes, the peak value of CL_H is higher than 30 dB/m and, simultaneously, the value of CL_F is still less than 0.4 dB/m. When fiber is in optimal HOM suppression, HOMs of the nodal S-ARFs with different cladding tubes are depicted in Figs. 9(c) and 9(d), demonstrating the coupling between core mode and core boundary mode is still efficient in the nodal S-ARF with 7 or 8 cladding tubes.

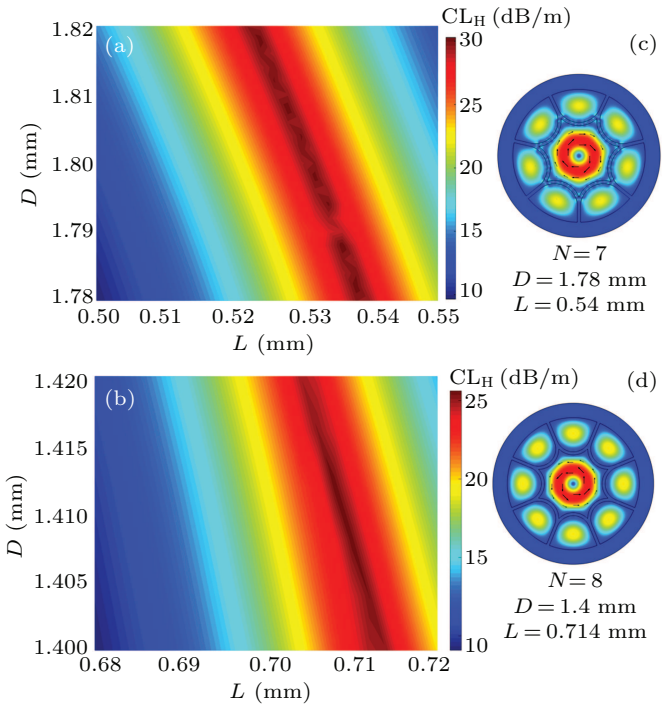


Fig. 9. In the nodal S-ARFs with 7 cladding tubes (a) and 8 cladding tubes (b), CL_H as functions of D and D_{core}. (c) The electric field distributions of HOM when N is 7; D is 1.78 mm and L is 0.54 mm. (d) The electric field distributions of HOM when N is 8; D is 1.4 mm and L is 0.714 mm.

3. Conclusion

This paper numerically investigated the index-induced mode couplings between core and cladding in THz ARFs. Based on the coupling of the higher-order mode in core and the fundamental mode in cladding tubes, ARFs can achieve a remarkable single-mode operation. The single-mode operation was proved can be obtained in ARFs, so long as satisfy the condition that the ratio of the cross-sectional area inside the cladding tubes to that of the central air core is kept at 0.46:1, and this area ratio also should be modified according to the shape and the number of cladding tubes. For the ARFs with 6 cladding tubes, when the form of the cladding tube is out of round, the area ratio of cladding tubes and core for optimal single-mode operation is slightly larger than 0.46:1; meanwhile, this area ratio is somewhat decreased when the number of cladding tubes is larger than 6. Besides, in the ARF with conjoint cladding tubes, the nodal core boundary is found can enhance the suppression on higher-order mode; accordingly, this paper proposed a single-mode ARF with conjoint semi-elliptical cladding tubes. Compared with the ARFs with nodeless cladding tubes, this nodal ARF has an almost identical fundamental mode loss but a larger higher-order mode loss.

References

[1] Zhong K, Shi W, Xu D, Liu P, Wang Y, Mei J, Yan C, Fu S and Yao J 2017 *Sci. China- Technol. Sci.* **60** 1801
[2] Yu F and Knight J C 2016 *IEEE J. Sel. Top. Quantum* **22** 146
[3] Belardi W and Knight J C 2013 *Opt. Express* **21** 21912
[4] Vincetti L 2009 *Opt. Fiber Technol.* **15** 398
[5] Poletti F 2014 *Opt. Express* **22** 23807
[6] Gao S F, Wang Y Y, Ding W, Jiang D L, Gu S, Zhang X and Wang P 2018 *Nat. Commun.* **9** 2828
[7] Nampoothiri A V V, Jones A M, Baumgart B, Washburn B R, Fourcade-dutin C, Mao C, Benabid F, Corwin K L, Alharbi M and Dadashzadeh N J O M E 2014 *Opt. Mater. Express* **2** 948
[8] Jones A M, Nampoothiri A V V, Ratanavis A, *et al.* 2011 *Opt. Express* **19** 2309
[9] Habib M S, Bang O and Bache M 2016 *Opt. Express* **24** 8429
[10] Gao S F, Wang Y Y, Liu X L, Ding W and Wang P 2016 *Opt. Express* **24** 14801
[11] Meng F C, Liu B W, Li Y F, Wang C Y and Hu M L 2017 *IEEE Photon. J.* **9** 1
[12] Yan S, Lou S, Wang X, Zhao T and Zhang W 2018 *Opt. Quantum Electron.* **50** 162
[13] Yu T Y, Liu X and Fan Z W 2018 *IEEE Photon. J.* **10** 1
[14] Kolyadin A N, Kosolapov A F, Pryamikov A D, Biriukov A S, Plotnichenko V G and Dianov E M 2013 *Opt. Express* **21** 9514
[15] Tuchin V V, Fedulova E V, Genina E A, Nazarov M M, Angeluts A A, Meglinski I V, Kitai M S, Sokolov V I and Shkurinov A P 2011 "Studying of dielectric properties of polymers in the terahertz frequency range", *Saratov Fall Meeting* 2011*: Optical Technologies in Biophysics and Medicine XIII*, 2012
[16] Anthony J, Leonhardt R, Leon Saval S G and Argyros A 2011 *Opt. Express* **19** 18470
[17] Islam M S, Cordeiro C M B, Franco M A R, Sultana J, Cruz A L S and Abbott D 2020 *Opt. Express* **28** 16089
[18] Ji J, Kong D, Ma T, He X, Chen Q and Wang L 2014 *Infrared and Laser Engineering* **43** 1909
[19] Pryamikov A D, Biriukov A S, Kosolapov A F, Plotnichenko V G and Dianov E M 2011 *Opt. Express* **19** 1441
[20] Huang X, Qi W, Ho D, Yong K T, Luan F and Yoo S 2016 *Opt. Express* **24** 7670
[21] Ventura A, Hayashi J G, Cimek J, Jasion G, Janicek P, Slimen F B, White N, Fu Q, Xu L, Sakr H, Wheeler N V, Richardson D J and Poletti F 2020 *Opt. Express* **28** 16542
[22] Yang J, Zhao J, Gong C, Tian H, Sun L, Chen P, Lin L and Liu W 2016 *Opt. Express* **24** 22454
[23] Alice C, Cristiano C and Marcos F J F 2018 *Fibers* **6** 43
[24] van Putten L D, Gorecki J, Numkam Fokoua E, Apostolopoulos V and Poletti F 2018 *Appl. Opt.* **57** 3953
[25] Uebel P, Günendi M C, Frosz M H, Ahmed G, Edavalath N N, Ménard J M and Russell P S J 2015 "A broad band robustly single mode hollow core PCF by resonant filtering of higher order modes", *Frontiers in Optics* 2015, Optical Society of America, San Jose, California 2015, FW6C.2
[26] Yu F, Xu M and Knight J C 2016 *Opt Express* **24** 12969
[27] Edavalath N N, Gunendi M C, Beravat R, Wong G K L, Frosz M H, Menard J M and St J R P 2017 *Opt. Lett.* **42** 2074
[28] Habib M S, Antonio Lopez J E, Markos C, Schulzgen A and Amezcua Correa R 2019 *Opt. Express* **27** 3824
[29] Yan S, Lian Z, Lou S, Wang X, Zhang W and Tang Z 2020 *Opt. Quantum Electron* **52** 269
[30] Sun S, Shi W, Sheng Q, Zhang G, Zhang Y, Yan Z and Yao J 2020 "Investigation of single mode anti resonant hollow-core THz fibers", 2020, Optical Society of America, San Jose, California 2020, 112791Y